Laboratory study of the electrical properties of Lutetian limestones in the [100 Hz-10 MHz] frequency range

Blaise Souffaché, Alain Tabbagh

Laboratory study of the electrical properties of Lutetian limestones in the [100 Hz- 10 MHz] frequency range

Blaise Souffaché, Alain Tabbagh
Sorbonne Université, CNRS, EPHE, UMR7619, Métis, 4 place Jussieu 75252, Paris, France

Abstract

Lutetian limestones have been widely used in historical monuments in the Paris Basin in the course of medieval and modern periods. Among the physical properties that can be used to assess the evolution of the limestones in situ in the buildings and their present health, the complex effective permittivity in the 10 kHz – 100 kHz frequency range is easy to measure and reflects the stone internal structure with also the dependence on the water content. To improve the knowledge about this property, a laboratory study on four samples collected in the relevant quarries has been undertaken along the 100 Hz – 10 MHz frequency range. Except close to zero water content, the observed results exhibit a quasi-absence of variation of the real effective permittivity with the water content. The frequency variation fairly fits with a model taking into account a Jonscher's decrease, a direct current conductivity, a high frequency dielectric permittivity and losses, and a relaxation phenomenon. When fitted by a Cole-Cole model, the magnitude of the corresponding relative permittivity change always stays close to 30 but the time constant varies from 1 to 0.1 μs as the water content increases.

Keywords

Effective dielectric permittivity of masonry stones, 100Hz – 10 MHz electromagnetic frequency range.

1-Introduction

Carbonate rocks account for an important portion of the sedimentary rocks present in the surficial layers of the Earth. They are often sufficiently porous and permeable to play a significant part in the processes of transfer and storage of groundwater or hydrocarbons, moreover, they have also played a determining role as materials used for construction since the beginnings of human society settlements. As for other sedimentary rocks there exist numerous publications dealing with electrical resistivity/conductivity as well as with their induced polarization at frequencies lower than 100Hz (Keller and Frischknecht 1966, Olhoeft 1985, Kenma et al. 2012); for higher 'intermediate' frequencies see Knight and Nur 1987.

In the perspective of civil engineering applications and for construction, sedimentary rocks deserve special attention because builders have to be able to evaluate the interest of their extraction *in situ* and then to follow over time their alteration in place in constructions. Restorers and building archaeologists have to assess their present health (Rozenbaum et al. 2007) and also intend to identify the choices that could have been those of the builders of ancient monuments (Souffaché et al. 2016). Good knowledge of the physical properties of these natural sedimentary materials is essential to achieve correct interpretations of the geophysical or non–destructive tests whatever investigation technique is used. In the present study the electrical properties are considered. They are expressed in terms of complex effective permittivity where the real component corresponds to the global electrical polarization and the imaginary component comprises both the direct current conductivity and dielectric losses.

This experimental study is limited to the Lutetian limestones of the Paris Basin the use of which as masonry stones has been very important in medieval and modern periods in spite of lateral variations of facies (Fronteau et al. 2010). A large number of quarries were operated on the whole Basin with numerous different techniques (Devos et al. 2010). The major component of these limestones is calcite with minor contents of quartz sand and clay minerals. These latter play an important role in the response to the application of an electric field due to

their high specific surface with ionic double layer (Stern and diffuse layers) surrounding the clay particles (Leroy and Revil 2009). The *in situ* measurements on ancient monuments (Souffaché et al. 2016) using a decimetric sized instrument showed over two different depth of investigation (approximately 10 and 20 cm) significant variations of both the real and imaginary components of the effective permittivity over the whole volume of masonry stones belonging to the facings. It is worth noting that in the old monuments, *i.e.* having exceeded a half–century of existence, the stone water content is constant beyond two to three centimeters whatever the weather conditions (Sass and Viles 2010). Where constructions are protected by roofs the weather fluctuations only leads to pellicle variations of the stone water content, conversely a significant water content would evidence a lack of protection. Moreover to get a global overview about the electrical properties of these stones and due to the huge impact of the water content on electrical properties of rocks and soils in general, it is inescapable to also investigate about its exact role.

The following experimental study is made at laboratory temperature (~ 20 °C) and does not consider the effect of the temperature, which *in situ* may vary from -10°C to 35°C at the masonry stone surface and may affect the ion mobility. Our work investigates the role of the liquid water content before paying particular attention to the frequency variations of the electrical properties of the four considered samples.

2-Materials and Methods

2-1 Samples

Our study is limited to limestones used in the Paris region for the construction of monuments. The materials studied in the laboratory are extracted from the same beds as those present in monuments: they are Lutetian limestones coming from the Saint Pierre Aigle (Aisne), Château Landon (Seine et Marne) and the Saint Maximin (Oise) (two samples referenced by 3B and 3E) quarries in the Paris Basin. The first two samples correspond to ‘strong’ masonry stones called ‘Liais’ by quarry workers, the two others to ‘light’ masonry stones called ‘Vergelé’ by quarry workers.

Their mineralogical composition is only prone to weak variations of facies with regard to the three major phases present in limestones: calcite 92 to 97%, quartz (silt) and phyllosilicates (clay) a few % (Blondeau et al. 1980). The ‘Vergelé’ samples correspond to the higher calcite content, their clay content is thus around 3%.However, there may be a difference in nature of the argillaceous phase between extraction sites: the clay can be pure illite, while smectite as well as interlayered clay add themselves in variable proportion to illite in another site. The difference between these two types of clay lies in the interfoliar cations: potassium for the illite, calcium and sodium for the smectite.

The samples, approximately weighting one kilogram, are first saturated by immersion in tap water of $\sigma w = 0.05 \pm 0.002$ Sm^{-1} conductivity during 48 h. Their open porosity, varying from 6 to 40% leads to absorption of water ranging from 20 to approximately 180 g. Effective permittivity measurements were made during free drying, each data acquisition being separated from the preceding by a weight loss of approximately 5 g. Last acquisitions at low water content were made after drying in an oven at 50° C for 24 hours.

2-2 measuring instrument

The measurement of the complex effective permittivity, ε, is carried out by means of a capacitive cell in which the limestone block of 160 x 160 x 19 mm^3 volume is placed between two metal plates and excited by an electric field with frequencies varying between 100 Hz and 10 MHz. Both the applied signal and the response are performed by a PSM 1735 vector multi-meter (Phase Sensitive Meter, NumetricQ Ltd) (Figure 1).

The instrument was first tested with moist clean sand, to assess its ability to follow low value and to compare the results with published calibration curves. We chose Fontainebleau

sand and made measurements during free drying at regular intervals of time. The results fit with the high frequency Law (Topp et al. 1980) in good agreement with the role played in permittivity value by the free water molecule rotation (~ 80).

2-3 Modelling

Looking at the frequency variation of the samples an empirical model has been chosen to describe the different behaviours successively observed. The general model fitting the data (see Figures below) comprises five terms (where ω is the angular frequency). The first corresponds to a Jonscher's decrease (Jonscher 1977) of the real part from the value ε_J, - the effective permittivity that must be added at 100 Hz (corresponding angular frequency ω_J) - to fit the datum. This decrease is characterized by the negative exponent, n. This global behaviour does not result from an identified physical phenomenon but of the number of possibly different phenomena and of their interactions. The second corresponds to the contribution of the dc conductivity, σ, to the imaginary part. The third corresponds to a relaxation which is described by the Cole-Cole empirical expression (Cole and Cole 1941); in this expression the relative permittivity step $\Delta\varepsilon$, the central time constant, τ, and the exponent, c, which characterizes the relaxation distribution around τ (there may exist several relaxations) intervene. The fourth and the fifth correspond to high frequency relative real, ε'_{HF}, and imaginary, ε''_{HF}, parts. The complete expression of the effective relative permittivity is thus written:

$$\varepsilon(\omega) = \varepsilon_j \left(\frac{\omega}{\omega_j}\right)^n - i\frac{\sigma}{\omega\varepsilon_0} + \frac{\Delta\varepsilon}{1+(i\omega\tau)^c} + \varepsilon'_{HF}(\omega) - i\varepsilon''_{HF}(\omega) \qquad (1)$$

The fit between the model effective permittivity and the measured permittivity values are controlled by the error expression, R:

$$R = \frac{1}{N}\sum_{i=1}^{N} \frac{\left|\varepsilon_i^{obs} - \varepsilon_i^{Th}\right|}{\varepsilon_i^{obs}} \qquad (2)$$

Where ε_i^{obs} is the observed complex effective permittivity, $\varepsilon_i^{Th}$the modelled one and N the number of frequency measurements.

3-Influence of the water content at fixed frequencies

It is common when considering the electrical/electromagnetic properties of rocks to first question the role of the volumetric water content, θ. The first characteristic that can be derived from this parameter is the porosity, φ, deduced from the value at saturation. As can be expected for the geological contexts Saint Maximin samples exhibit high porosities, greater for 3B (0.411) than for 3E (0.331); Saint Pierre - Aigle sample a medium porosity (0.189) and Château Landon the smallest ones (0.0664).

The variations of the real part of the effective permittivity are presented in Figures 2, 3, 4 and 5. For the Chateau Landon and Saint Pierre Aigle samples with lower porosities the scattering is significant but it must be observed that while gently increasing at 1 kHz, the values are quasi-constant above θ=0.02 for 10 kHz and 100 kHz.. For Saint Maximin samples with higher porosities the increase is sensible until θ=0.09. Contrary to the 1 kHz increase, the 10 KHz and 100 kHz variation are very small. As detailed below, this stability results from a compensation effect between higher ε_J values and more negative Jonscher's exponent n.

4-Results of the frequency dependence modelling

4-1 Chateau Landon

In this very low porosity sample, φ=0.0664, the volumetric water content range of variation is limited. The frequency behavior of the effective relative permittivity for different θ values is illustrated in Figure 6, where the measured values are in black dots, the real part of the fitting curve in red and its imaginary part in blue. The main observable feature is the

presence of a relaxation phenomenon that moves to higher frequency as the water content increases (Figure 10). The conductivity effect is observable from 0.0333 water content but not at 0.0218 due to the limits of the instrument. The slopes fitted by a Jonscher's expression also manifest themselves at upper water contents. The different modelling parameters are given in Table 1 for the whole water content extent feasible with this sample. As the water content increases the Jonscher's exponent, *n*, decreases from -0.1 to -0.5, ε_J, σ and ε'_{HF} increases, $\Delta\varepsilon$ is scattered around 22 but slightly decreasing, *c* lies in the [0.74 .88] interval and τ decreases. The τ variation is illustrated in Figure 10 together with the other samples to facilitate comparison. It can be approximated by a linear Log-Log variation and then follows a law of power with a -1.12 rate with a resulting 0.89 Pearson's correlation coefficient (for 6 observations).

4-2 Saint Pierre Aigle

Figure 7 demonstrates the measured and modelled results of real and imaginary relative electric permittivity for four different water content levels (measurements in black dots, curve fitting the real part in red, curve fitting the imaginary part in blue) of the relative effective permittivity. Again for the lower value of θ the conductivity influence on the imaginary part cannot be observed. For higher values it generates a linear decrease of the imaginary part but of significantly greater magnitude than the real part in the lower portion of the frequency range. Here again the Jonscher's decrease, not observable for lower θ values, exhibits increasing presence at larger water contents. For this sample the existence of a distinct relaxation phenomenon again is the major feature of the curves.

Table 2 gives the values of the different model parameters along the widest water content range possible for this sample. The Jonscher's exponent decreases from 0 to -1, ε_J, σ and ε'_{HF} increases, $\Delta\varepsilon$ slightly decreases, *c* lies in the [0.62, 0.88] interval and τ decreases. The τ variation, illustrated in Figure 10, follows here a law of power with a -1.26 rate with a 0.99 resulting Pearson's correlation coefficient (for 11 observations).

4-3 Saint Maximin sample 3B

This first sample of Saint Maximin presents the greatest porosity, φ=0.411, the extent in water content variations is thus large and the permittivity reaches very high values as illustrated in Figure 8. The numerical values of the modelling parameters are presented in Table 3. With this sample it has been possible to obtain a very low water content where the frequency variation can be interpreted as simple decrease following a τ=3.6 ms relaxation (the corresponding frequency, 44 Hz, lies outside the measurement interval). For the other values one clearly observes the conductivity influence on the imaginary part. The Jonscher's exponent decreases from -0.72 to -1.02, ε_J exhibits a maximum at θ=0.279, σ reaches a plateau for the higher water contents, ε'_{HF} regularly increases, $\Delta\varepsilon$ slightly decreases, *c* lies in the [0.76, 1] interval and τ regularly decreases. The τ variation is illustrated in Figure 10, contrary to the preceding samples the curve is not approximately linear but incurved for higher water contents.

4-4 Saint Maximin sample 3E

This second sample of the same quarry has a lesser porosity, φ=0.331, and its behavior is somewhat different as illustrated in Figure 9 and Table 4. The Jonscher's exponent exhibits a larger interval, [-.14, -1.25], the ε_J and σ values reach greater values, *c* and τ are comparable but $\Delta\varepsilon$ is slightly higher. As for the other Saint Maximin sample, the τ variation (Figure 10) is incurved and tends to stabilize around 0.1 µs for the higher water contents.

5-Discussion

In the measured frequency range the electrical and electromagnetic properties cannot be deduced from simple mixing laws based on the constituent high frequency permittivity: 2.2 for calcite (crystal polarization) and 80 for water (rotation of free molecules). The arrangement and shapes of the grains, the pore networks and the presence of clay platelets generate complex polarization phenomena. High permittivity values have theoretically (Tabbagh et al. 2009) been

modelled, but laboratory experiments are required to identify the phenomena acting in a given frequency range and to be able to interpret *in situ* measurements. One first observed strong changes of the permittivity values when the volumetric water content increases from 0 to 0.02 (for low porosity samples) or 0.08 (for high porosity samples) followed by limited variations. In monuments masonry stones are protected by a roof and their volumetric water content, which is stable in relation to the average air humidity, stays in the 0.05 – 0.06 interval whatever the weather conditions. An increase of water content would indicate a degradation of the stones observable with the imaginary part (conductivity increase). In good conditions one can expect that the impact of moisture change on the real part of the effective permittivity will be limited whereas the structural characteristics of the solid grains nature and arrangement will play a more significant role and make the identification of masonry stone and facies changes quite easy.

Above around 0.02 water content the mains characteristics of the frequency dependence of the complex effective permittivity are: (1) a global decrease against the frequency and (2) the presence of a relaxation phenomenon. As expected the decrease of the imaginary part is inversely proportional to the direct current conductivity value. The decrease of the real part can be described by a Jonscher's law that corresponds to a wide distribution of small relaxation phenomena. For all the samples the easily identifiable relaxation corresponds to time constants varying from 1 to 0.1 µs as the water content increases. This relaxation exists for very small water content and the corresponding permittivity step, $\Delta\varepsilon$, does not significantly change with the water content. Consequently these two characteristics must probably be related to the presence of the electrical double layer (EDL) at the surface of clay platelets. The surficial ion quantity does not change but in absence of free water, with bounded water only, their displacement is slow, and as the free water content increases their displacement is facilitated. For this relaxation, the underlying process would then be the EDL polarization.

All these experimental data will be put in regard to the general classification of the polarization phenomena (Kemna et al. 2012, Loewer et al. 2017, Niu et al. 2020). However this will be a difficult task as the Jonscher's type decreases of the real parts with frequency correspond to large distributions of time constants and possibly to different polarization processes. Interestingly it can be described by only two empirical parameters ε_J and n the contradictory effect of which explains at fixed frequency the observed limited dependence on the water content.

6-Conclusion

As regards the measuring point of view, the present experimental study first confirms that in the considered frequency range the real part of the permittivity can be high, far higher than the one observed in the high frequency ground penetrating radar range. It can override the conductivity response expressed by the imaginary part and both components must be taken into account when measuring. This observation well agrees with the publications dealing with the 'intermediate' frequency range (Tabbagh et al. 2021).

Concerning the stones themselves, we lack comparison with other types of sedimentary and not sedimentary rocks, but the attribution to the clay fraction of the relaxation observed for these Lutetian limestones is proposed. A greater panel of experiments with deeper characterization remains now to be undertaken in order to better assess this hypothesis.

Acknowledgements

The work was achieved with the contribution of Métis (UMR7619, Sorbonne Université) funds. In-kind contribution for stone characterization was provided by Dr Jean-Pierre Gély (Université Paris 1 Panthéon-Sorbonne). We warmly thank the Associate Editor and the two reviewers for their constructive criticism and suggestions.

References

Blondeau A., Cavelier C., Labourguigne J., Mégnien C., Mégnien F., 1980. Eocène moyen, *in Synthèse géologique du bassin de Paris*, mémoire BRGM n°101, chapitre 12, p 374.

Cole K. S., Cole R. H., 1941. Dispersion and Absorption in Dielectrics 1. Alternating Current Characteristics. *Journal of Chemical Physics*, 9, 341-351.

Devos A., Fronteau G., Lejeune O., Sosson C., Chopin E., Barbin V., 2010. Influence of geomorphological constraints and exploitation techniques on stone quarry spatial organization. Example of Lutetian underground quarries in Reims, Laon and Soisson areas. *Engineering Geology*, 115, 268-275.

Fronteau G., Moreau C., Thomachot C., Barbin V., 2010. Variability of some Lutetian building stones from the Paris Basin, from characterization to conservation. *Engineering. Geology*. 115, 158-166.

Jonscher A.K., 1977. The ' universal ' dielectric response. *Nature*, Vol 267, 673-679.

Keller G.V. and Frischknecht F.C., 1966. Electrical Methods in Geophysical Prospecting. Pergamon Press, Oxford.

Kemna A., Binley A., Cassiani G., Niederleithinger E., Revil A., Slater L., Williams K. H., Flores Orozco A., Haegel F-H., Hördt A., Kruschwitz S., Leroux V., Titov K., Zimmermann E., 2012. An overview of the spectral induced polarization method for near-surface applications. *Near Surface Geophysics*, 10, 453–468.

Knight R. J., Nur A., 1987. The dielectric constant of sandstones, 60 kHz to 4 MHz. *Geophysics*, 52-5, 644-654.

Leroy P., Revil A., 2009. A mechanistic model for the spectral induced polarization of clay minerals. *Journal of Geophysical Research*, 114, B10202.

Loewer M., Gunther T., Igel J., Kruschwitz S., Martin T., Wagner N., 2017. Ultra-broad-band electrical spectroscopy of soils and sediments - a combined permittivity and conductivity model. Geophysical Journal International, 210, 1360-1373.

Niu Q., Zhang C., Prasad M., 2020. A Framework for Pore-Scale Simulation of Effective Electrical Conductivity and Permittivity of Porous Media in the Frequency Range from 1 mHz to 1 GHz. *Journal of Geophysical Research*, doi. 10.1029/2020JB020515Olhoeft G.R., 1985. Low-frequency electrical properties. *Geophysics.* 50-12, 2492-2503.

Rozenbaum O., Le Trong E., Rouet J. L., Bruand A., 2007. 2D – image analysis: A complementary tool for characterizing quarry and weathered building limestone. *Journal of Cultural Heritage*, 8, 151-159.

Sass O., Viles H. A., 2010. Wetting and drying of masonry walls: 2D resistivity monitoring of driving rain experiment on historic stonework in Oxford, UK. *Journal of Applied Geophysics*, 70, 72-83.

Souffaché B., Kessouri P., Blanc P., Tabbagh A., 2016. First investigations of in situ electrical properties of limestone blocks of ancient monuments. *Archaeometry*, 58-5, 705-721.

Tabbagh A., Cosenza P., Ghorbani A., Guérin R., Florsch N., 2009. Modelling of Maxwell-Wagner Induced Polarization Amplitude for Clayey Materials. *Journal of Applied geophysics*, 67-2, 109-113.

Tabbagh A., Rejiba F., Finco C., Schamper C., Souffaché B., Camerlynck C., Thiesson J., Jougnot D., Maineult A., 2021. The case for considering polarization in the interpretation of electrical and electromagnetic measurements in the 3 kHz to 3 MHz frequency range. *Surveys in Geophysics*, 42-2, 377-397. doi: 10.1007/s10712-020-09625-1

Topp G. C., Davis J. L., Annan A. P., 1980. Electromagnetic determination of soil water content: measurements in coaxial transmission lines. *Water Resources Research*, 16, 574-582.

Figure captions

Figure 1 Instrumentation: capacitive cell and PSM vector multi-meter. The limestone blocks are 160 x 160 x 19 mm^3 sized.

Figure 2. Real part of the effective permittivity of the Chateau Landon sample as a function of water content at 1 kHz, 10 kHz and 100 kHz.

Figure 3. Real part of the effective permittivity of the Saint Pierre Aigle sample as a function of water content at 1 kHz, 10 kHz and 100 kHz.

Figure 4. Real part of the effective permittivity of the Saint Maximin 3B sample as a function of water content at 1 kHz, 10 kHz and 100 kHz.

Figure 5. Real part of the effective permittivity of the Saint Maximin 3E sample as a function of water content at 1 kHz, 10 kHz and 100 kHz.

Figure 6: Chateau Landon sample: frequency dependence of the relative permittivity for different volumetric water contents. Measured data in black dots, theoretical curves in red for the real component and in blue for the imaginary component. R is the residual relative error.

Figure 7: Saint Pierre Aigle sample: frequency dependence of the relative permittivity for different volumetric water contents. Measured data in black dots, theoretical curves in red for the real component and in blue for the imaginary component. R is the residual relative error.

Figure 8: Saint Maximin 3B sample: frequency dependence of the relative permittivity for different volumetric water contents. Measured data in black dots, theoretical curves in red for the real component and in blue for the imaginary component. R is the residual relative error.

Figure 9: Saint Maximin 3E sample: frequency dependence of the relative permittivity for different volumetric water contents. Measured data in black dots, theoretical curves in red for the real component and in blue for the imaginary component. R is the residual relative error.

Figure 10: Four samples relationships between the relaxation time constant and the volumetric water content: for Château Landon (brown crosses) the power law slope is -1.12, for Saint Pierre Aigle sample (green diamonds) the power law slope is -1.28, for Saint Maximin 3B (red triangles) and 3E (black triangles) samples, the variations show a curvature and do not fit with a power law.

Table captions

Table 1: Numerical values of the model parameters obtained by fitting with the whole water content range for Chateau Landon sample.

Table 2: Numerical values of the model parameters obtained by fitting with the whole water content range for Saint Pierre Aigle sample.

Table 3: Numerical values of the model parameters obtained by fitting with the whole water content range for Saint Maximin 3B.

Table 4: Numerical values of the model parameters obtained by fitting with the whole water content range for Saint Maximin 3E.

Figure captions

Figure 1 Instrumentation: capacitive cell and PSM vector multi-meter. The limestone blocks are 160 x 160 x 19 mm^3 sized.

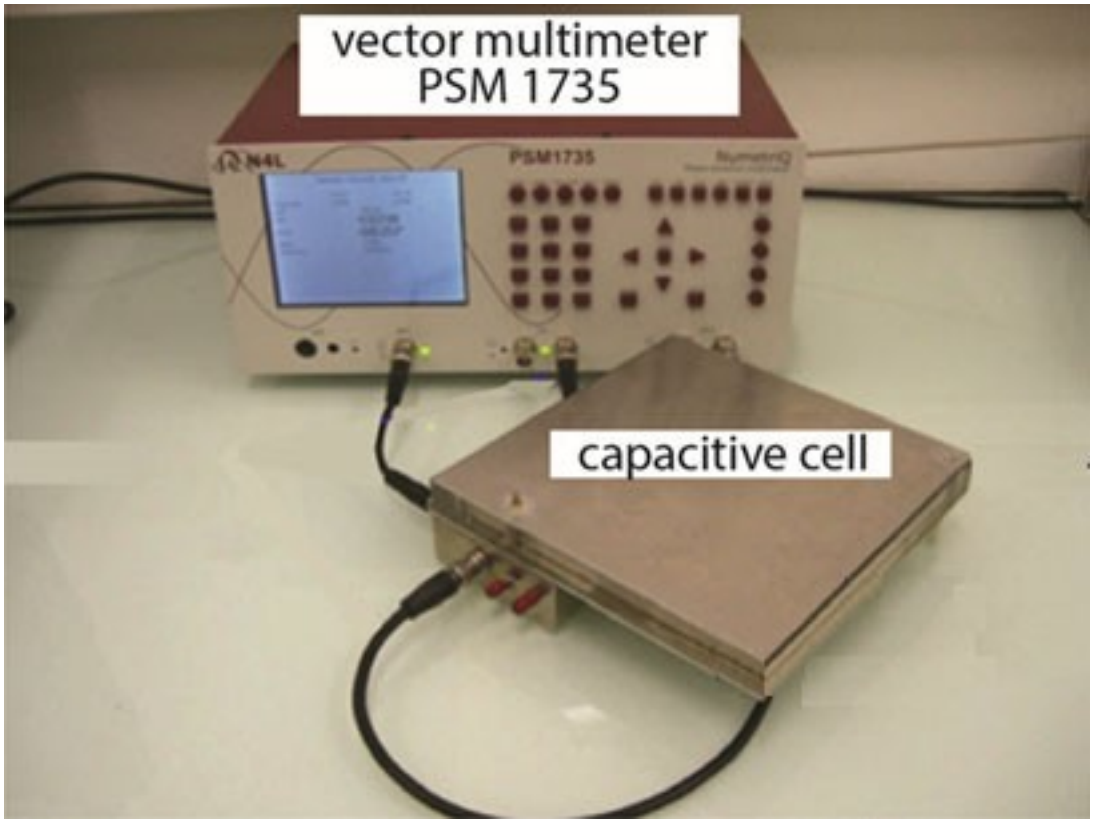

Figure 2. Real part of the effective permittivity of the Chateau Landon sample as a function of water content at 1 kHz, 10 kHz and 100 kHz.

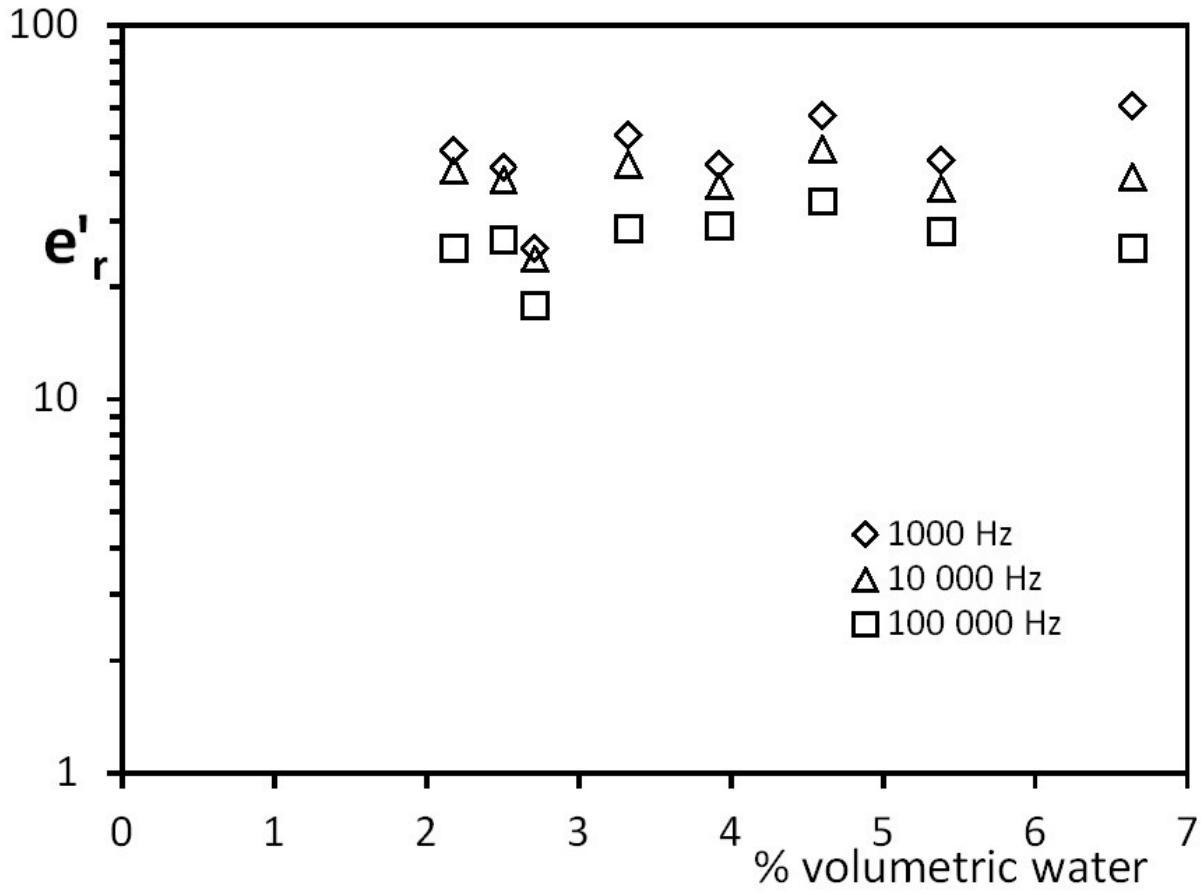

Figure 3. Real part of the effective permittivity of the Saint Pierre Aigle sample as a function of water content at 1 kHz, 10 kHz and 100 kHz.

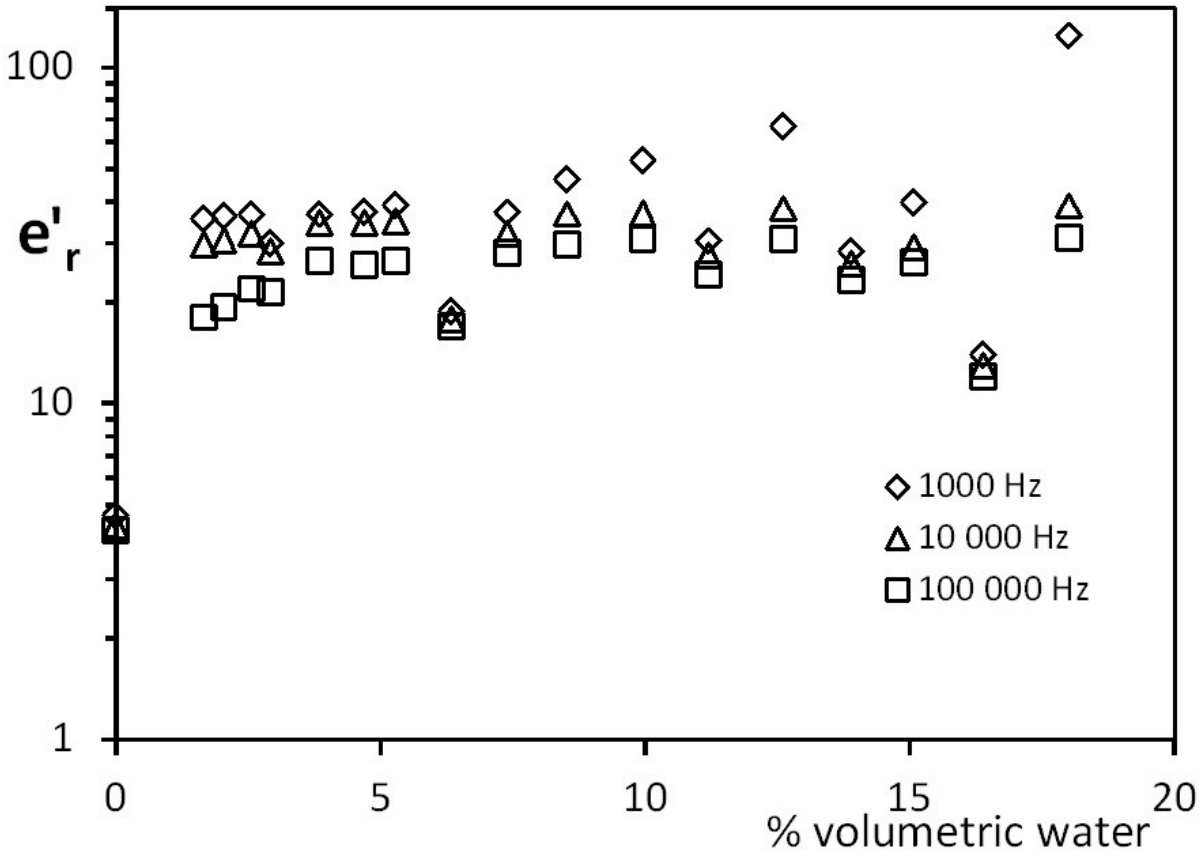

Figure 4. Real part of the effective permittivity of the Saint Maximin 3B sample as a function of water content at 1 kHz, 10 kHz and 100 kHz.

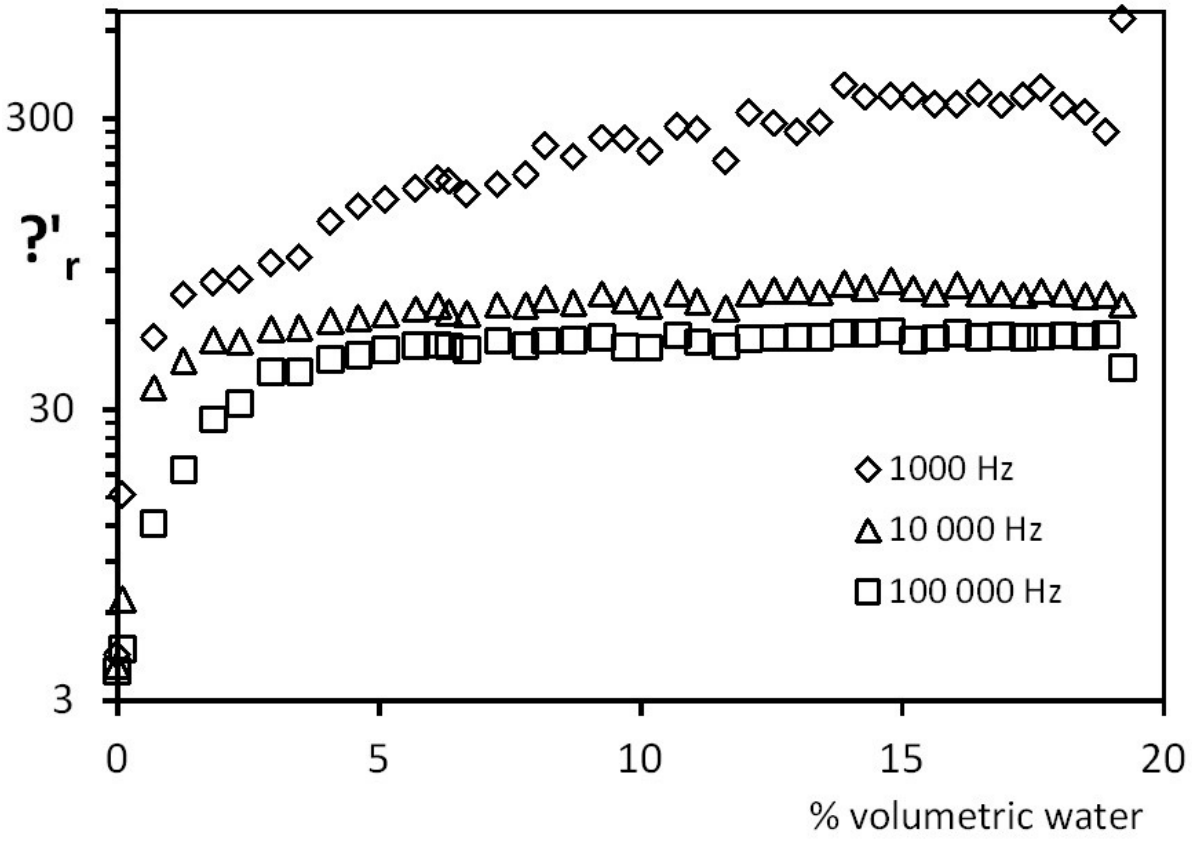

Figure 5. Real part of the effective permittivity of the Saint Maximin 3E sample as a function of water content at 1 kHz, 10 kHz and 100 kHz.

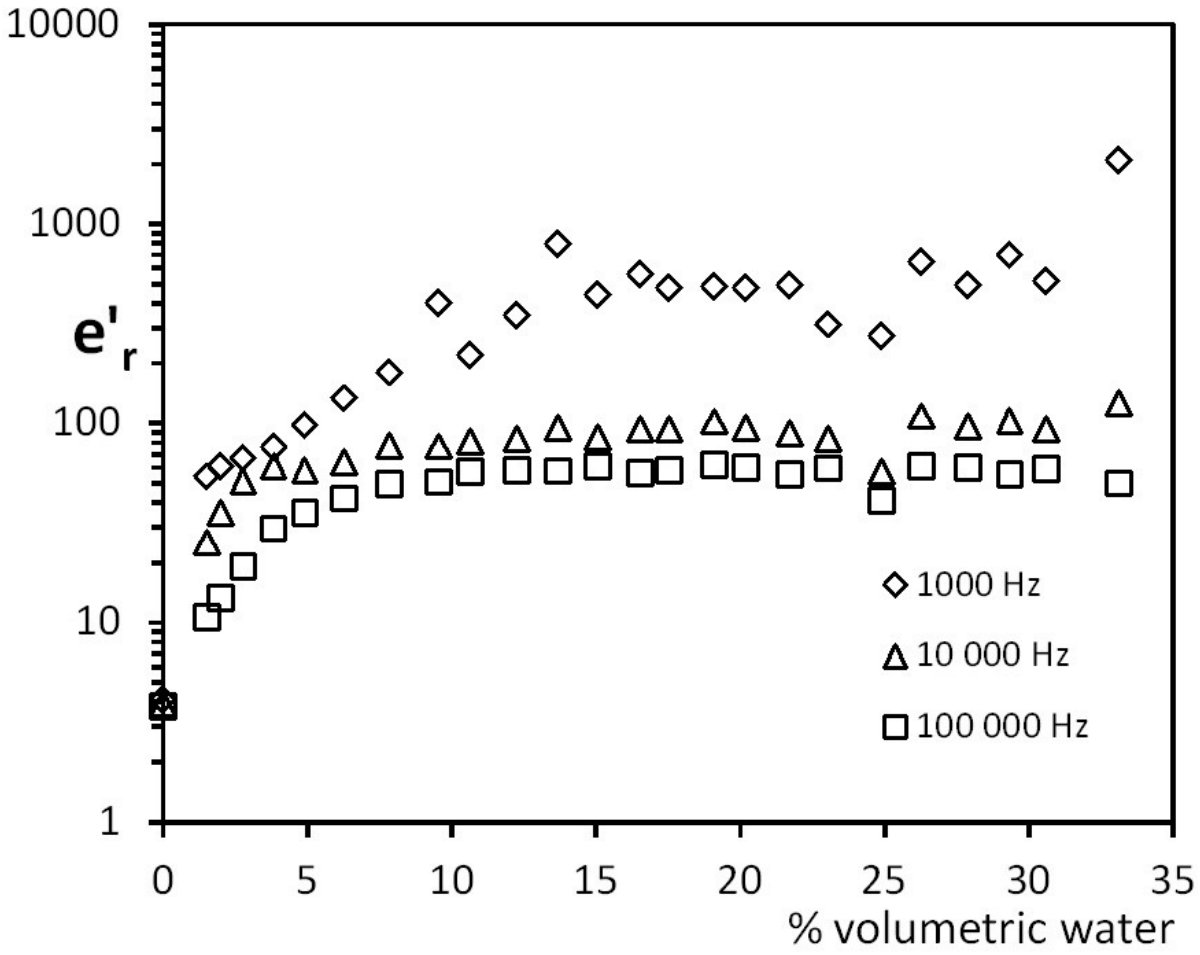

Figure 6: Chateau Landon sample: frequency dependence of the relative permittivity for different volumetric water contents. Measured data in black dots, theoretical curves in red for the real component and in blue for the imaginary component. R is the residual relative error.

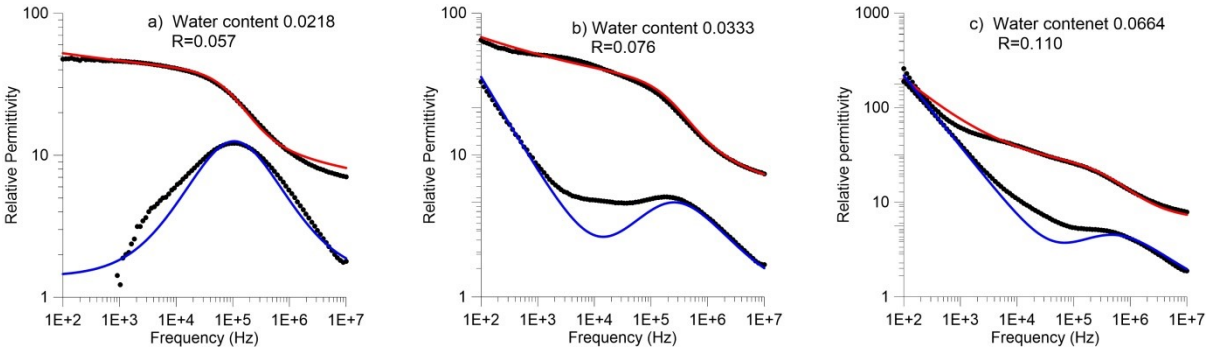

Figure 7: Saint Pierre Aigle sample: frequency dependence of the relative permittivity for different volumetric water contents. Measured data in black dots, theoretical curves in red for the real component and in blue for the imaginary component. R is the residual relative error.

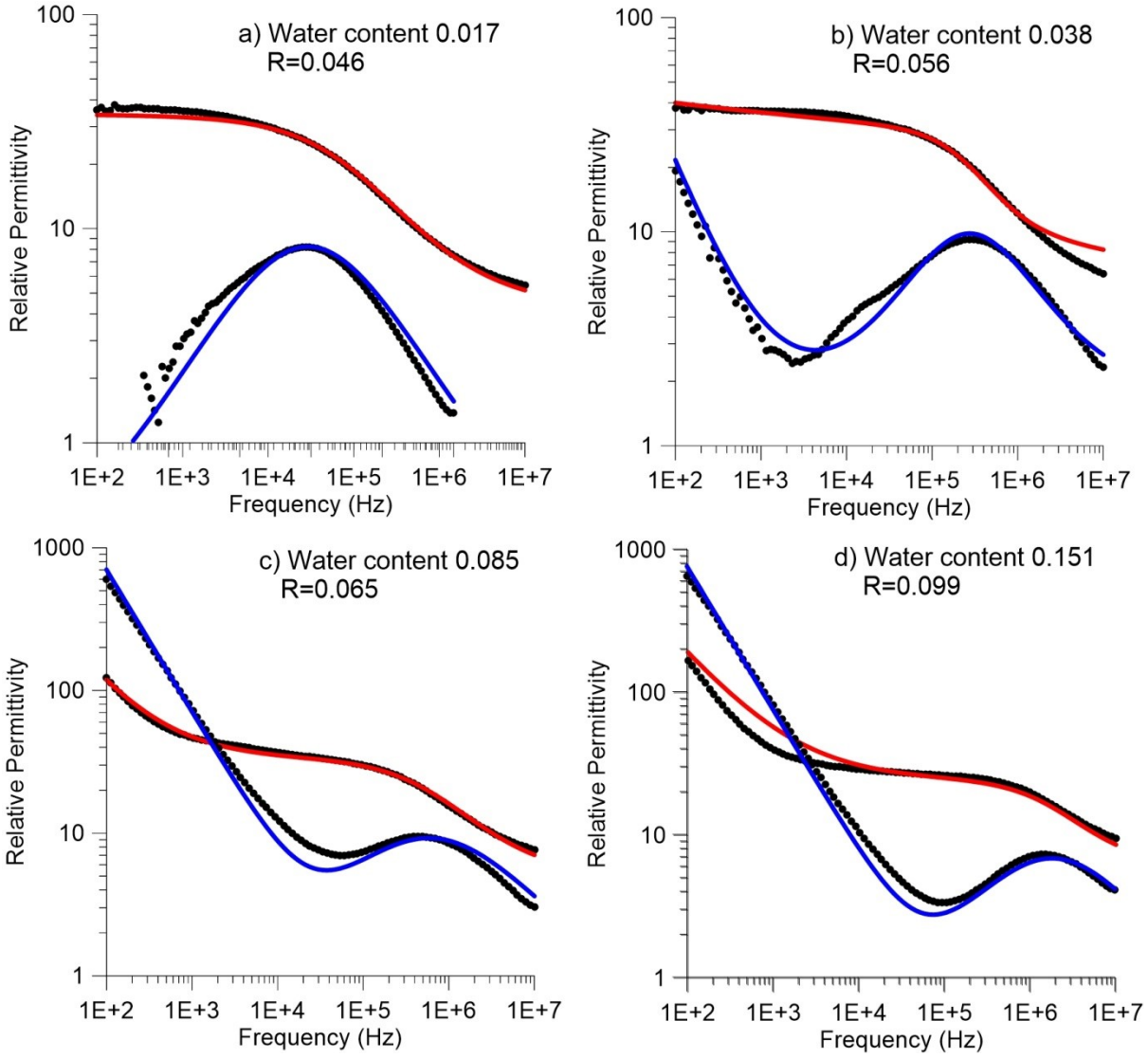

Figure 8: Saint Maximin 3B sample: frequency dependence of the relative permittivity for different volumetric water contents. Measured data in black dots, theoretical curves in red for the real component and in blue for the imaginary component. R is the residual relative error.

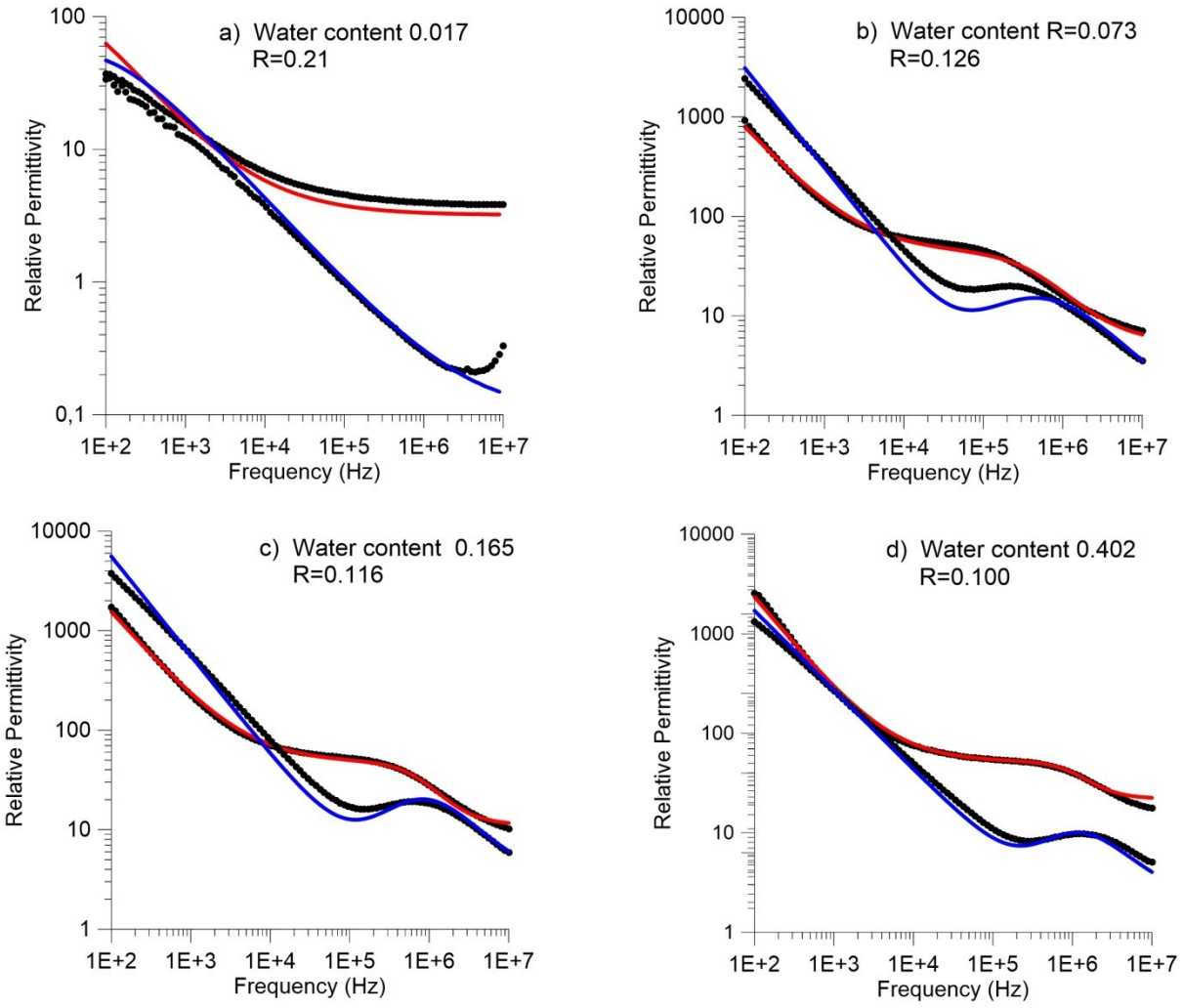

Figure 9: Saint Maximin 3E sample: frequency dependence of the relative permittivity for different volumetric water contents. Measured data in black dots, theoretical curves in red for the real component and in blue for the imaginary component. R is the residual relative error.

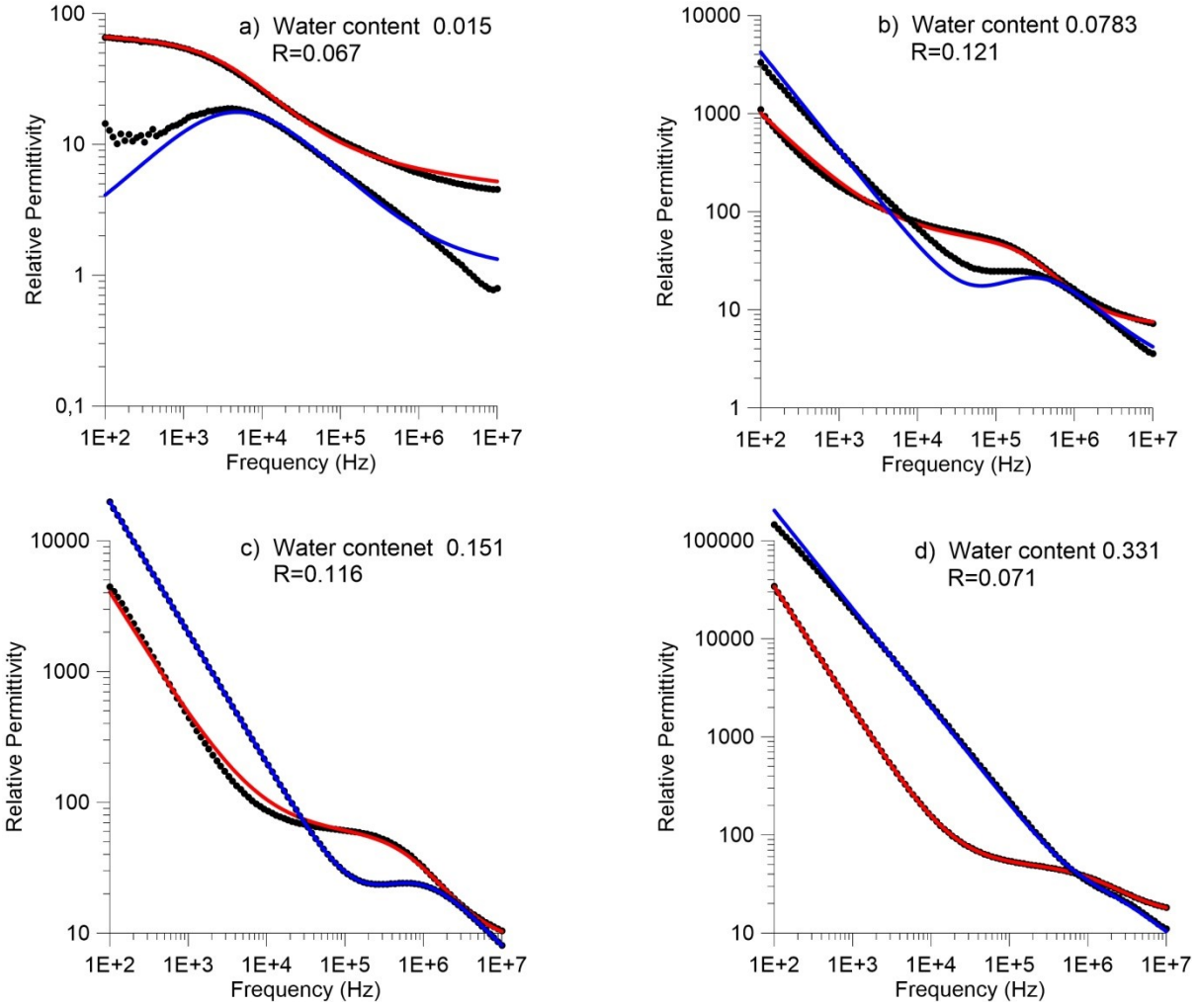

Figure 10: Four samples relationships between the relaxation time constant and the volumetric water content: for Château Landon (brown crosses) the power law slope is -1.12, for Saint Pierre Aigle sample (green diamonds) the power law slope is -1.28, for Saint Maximin 3B (red triangles) and 3E (black triangles) samples, the variations show a curvature and do not fit with a power law.

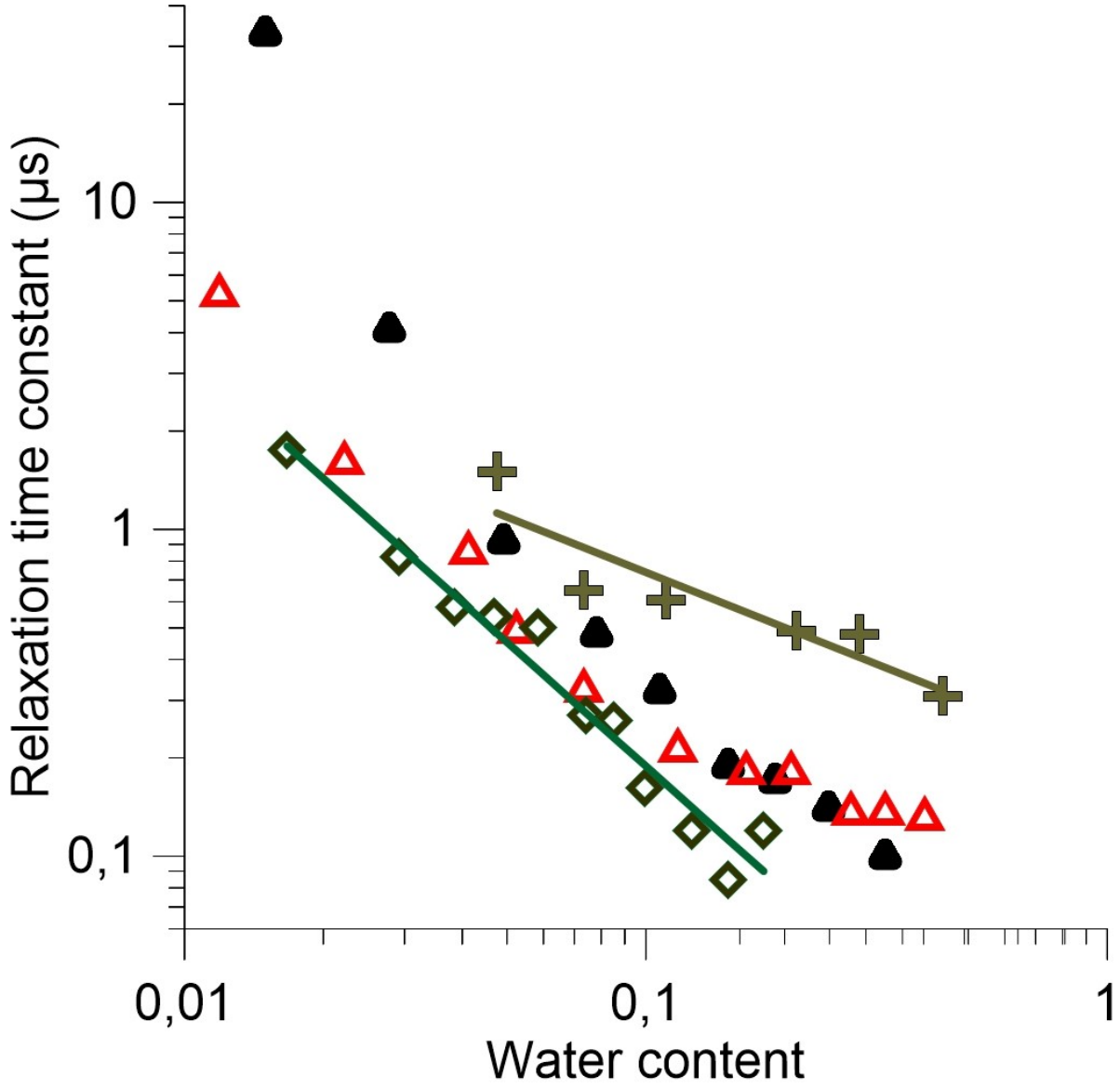

Table captions

Table 1: Numerical values of the model parameters obtained by fitting with the whole water content range for Chateau Landon sample.

θ	n	ε_J	σ ($\mu S/m$)	ε'_{HF}	ε''_{HF}	$\Delta\varepsilon$	c	τ (μs)
0.0218	-0.135	22	0	3.40	1.4	27	0.88	1.50
0.0271	-0.18	14	0	3.60	0.7	14.5	0.74	0.65
0.0333	-0.22	41	1.17	3.75	1.0	23	0.84	0.61
0.0461	-0.25	50	0.48	3.9	1.3	27	0.80	0.49
0.0539	-0.25	42	0.93	4.2	1.0	22	0.75	0.48
0.0664	-0.54	180	7.3	6.3	0.9	18	0.78	0.31

Table 1

Table 2: Numerical values of the model parameters obtained by fitting with the whole water content range for Saint Pierre Aigle sample.

θ	n	ε_J	σ ($\mu S/m$)	ε'_{HF}	ε''_{HF}	$\Delta\varepsilon$	c	τ (μs)
0.0167	0	1.0	0	3.22	0.3	30	0.62	1.75
0.0292	0	2.0	0	3.42	0.3	25	0.70	0.82
0.0384	-0.12	16	0.1	4.0	1.8	20	0.86	0.58
0.0469	-.15	15	0.17	3.6	0.3	24	0.80	0.54
0.0582	-.30	29	0.54	5.15	1.3	20	0.78	0.50
0.0740	-.40	27	0.62	7.10	1.32	20.5	0.85	0.27
0.0853	-.79	85	3.9	4.8	0.4	29	0.69	0.26
0.0995	-.81	241	9,7	3.9	0.3	28	0.68	0.162
0.126	-.88	438	15.0	7.1	1.2	22	0.79	0.12
0.151	-.71	167	42.0	5.9	0.3	19	0.76	0.085
0.180	-.944	1150	45.0	10.2	1.2	18.2	0.88	0.12

Table 2

Table 3: Numerical values of the model parameters obtained by fitting with the whole water content range for Saint Maximin 3B.

θ	n	ε_J	σ (μS/m)	ε'_{HF}	ε''_{HF}	$\Delta\varepsilon$	c	τ (μs)
0.0017	0	0	0	3.2	0.1	180	0.66	3600
0.0222	-0.72	219	3.8	4.15	0.	30	0.76	1.6
0.0414	-0.85	280	5.2	6.1	0.75	38	0.85	0.85
0.0523	-0.65	300	5.6	5.4	0.80	37	0.82	0.485
0.0732	-0.87	750	17.2	5.0	0.2	40	0.79	0.32
0.117	-0.85	1000	26.	8.2	1.0	38	0.89	0.21
0.165	-0.90	1500	31.	11.0	2.5	37	0.95	0.185
0.207	-0.89	2000	44.	11.0	2.5	38	0.89	0.18
0.279	-0.96	3100	69.	15.	3.5	37	0.92	0.135
0.330	-1.02	2800	63.	18.	2.0	35	0.97	0.135
0.402	-0.97	2300	61.	22.	2.0	30	1.0	0.13

Table 3

Table 4: Numerical values of the model parameters obtained by fitting with the whole water content range for Saint Maximin 3E.

θ	n	ε_J	σ (μS/m)	ε'_{HF}	ε''_{HF}	$\Delta\varepsilon$	c	τ (μs)
0.015	-0.14	11	0	2.9	1.1	54	0.70	33.0
0.0278	-0.23	37	0.39	3.2	1.3	44	0.87	4.1
0.0491	-0.85	460	15.0	6.1	0.95	43	0.84	0.92
0.0783	-0.80	960	23.5	6.9	2.0	44	0.87	0.48
0.107	-0.87	1500	34.0	6.4	2.2	48	0.79	0.32
0.151	-0.97	4000	110.	7.7	1.9	52	0.82	0.19
0.191	-0.94	4000	106.	8.3	2.1	53	0.81	0.17
0.331	-1.25	34000	1130.	14.5	2.0	35	0.80	0.10

Table 4